Earthquake (2025) Volume 3 Issue 2 ISSN: 3029-1550 (O)
doi: 10.59429/ear.v3i2.9744

RESEARCH ARTICLE

Coseismic Displacement Field of the 28 March 2025 Myanmar Earthquake (Mw 7.7) Derived From InSAR

Lotfollah Emadali*, Sasan Motaghed

Department of Civil Engineering, Faculty of Engineering, Behbahan Khatam Alanbia University of Technology, Behbahan, Iran

*** Corresponding author:** Lotfollah Emadali,emadali@bkatu.ac.ir

Abstract

This study investigates the surface coseismic deformation caused by the 28 March 2025 Myanmar earthquake (Mw 7.7) using Interferometric Synthetic Aperture Radar (InSAR) technique with Sentinel-1A data. The earthquake, occurring along the Sagaing Fault, resulted in significant ground displacement, impacting infrastructure and communities. InSAR analysis reveals detailed deformation patterns, quantified through interferograms, multi-look processing, unwrapped phase data, and displacement maps. Results indicate a rupture zone extending approximately 110 km, with maximum subsidence of -0.82 meters and uplift of 0.18 meters, along the Line Of Sight of satellite (LOS). These findings correlate with observed structural damage and provide insights into the fault's slip distribution. The earthquake's shallow depth (about 10 km) and strike-slip faulting produced violent ground shaking (Modified Mercalli Intensity IX), which, when coupled with subsidence, exacerbated damage to structures, especially those built on soft soils or with substandard construction practices common in the region. This study demonstrates the effectiveness of InSAR in assessing earthquake-induced deformation, offering valuable data for seismic hazard assessment, disaster response, and long-term resilience planning in this vulnerable region. Integrating satellite-based remote sensing with macroseismic data contributes to a comprehensive understanding of seismic events, supporting improved risk mitigation strategies.

Keywords: earthquake deformation; InSAR; Sagaing fault; disaster assessment

1. Introduction

The March 28, 2025, Myanmar earthquake (Mw 7.7) represents one of the most devastating seismic events in Southeast Asia's modern history, offering critical insights into regional tectonics and disaster impacts. Striking near the Sagaing-Mandalay border at a shallow depth of 10 km, the earthquake caused catastrophic damage across central Myanmar, with cascading effects on neighboring countries. This event underscores the persistent seismic hazard along the Sagaing Fault, a major right-lateral strike-slip structure accommodating the oblique convergence between the Indian and Eurasian plates[1-5]. Historical records reveal recurrent seismicity in this region, including the 1930 Bago (M 7.3) and 2012 Thabeikkyin (M 6.8) earthquakes, highlighting the fault's capacity for generating high-magnitude events [6-8].

ARTICLE INFO
Received: 21 April 2025|Accepted: 22 May 2025|Available online: 30 May 2025

CITATION
L. Emadali, S. Motaghed. Coseismic Displacement Field of the 28 March 2025 Myanmar Earthquake (Mw 7.7) Derived from InSAR. *Earthquake*. 2025; 3(2): 9744.doi: 10.59429/ear.v3i2.9744

The Sagaing Fault, extending ~1,200 km through Myanmar, slips at ~18 mm/yr, as quantified by GPS measurements. This fault system partitions strain from the India-Sunda plate boundary, with stress accumulation leading to periodic release through major earthquakes [9-11]. The 2025 event ruptured a segment previously identified as a seismic gap in satellite geodesy studies [12]. Paleoseismic investigations by Wang et al. (2014) identified recurrence intervals of 500–700 years for M ≥7.5 earthquakes along this fault, aligning with the 2025 rupture's characteristics[9-10]. The National Institute of Natural Disaster Prevention's Earthquake Disaster Research Center analyzed co-seismic deformation using 24 Sentinel-2 satellite images (March 7–20 and March 30–April 1, 2025) with Caltech's Cosi-Corr software. Results indicate a right-lateral strike-slip earthquake with a 440 km surface rupture. Maximum horizontal displacement reached ~6 meters near Mandalay, Myanmar (epicenter), averaging 3–4 meters. These findings support earthquake disaster assessments and seismic mechanism studies.

The earthquake's human toll was devastating, with over 3,500 confirmed fatalities reported by the World Health Organization (WHO) as of April 7, alongside approximately 5,000 injuries and more than 200 people missing. Satellite data analysis revealed extensive displacement, with over 100,000 people forced to evacuate affected regions in Mandalay and Sagaing. Critical infrastructure suffered catastrophic damage, including the collapse of culturally significant landmarks like Mahamuni Pagoda in Mandalay and the strategic Ava Bridge in Sagaing, while 60% of residential structures in the epicentral zone were destroyed. The economic impact reached staggering proportions, with preliminary estimates suggesting losses between $10 billion and $20 billion—a figure surpassing Myanmar's annual GDP. Seismic effects extended across approximately 500,000 km², with perceptible shaking reported as far as Chiang Mai (Thailand), northeastern India, and southwestern China[6,1]. The main shock triggered intense aftershock activity, including 127 events exceeding M 4.0 within 72 hours, notably a potent M 6.4 tremor occurring just ten minutes after the initial rupture[11-14].

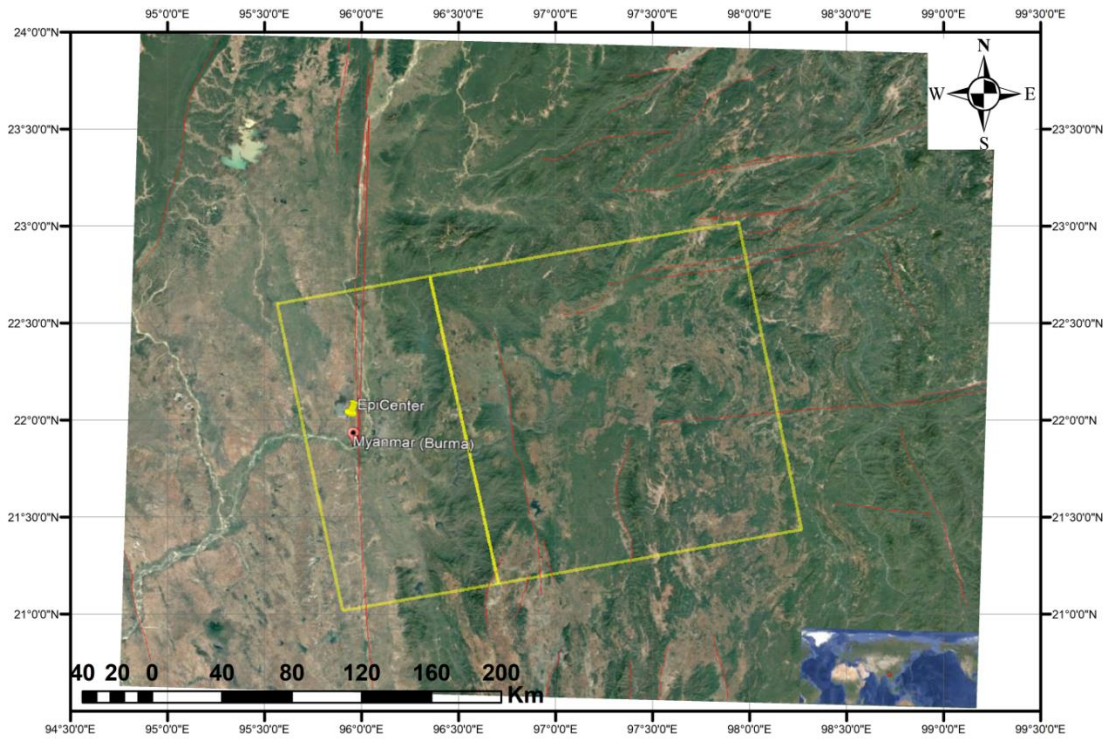

Figure 1. The Google Earth image of the study area (Myanmar): The yellow rectangle represents the footprint of Sentinel-1A images in the Ascending orbit of satellite; the epicenter of earthquake has been shown at the figure.

The epicenter coordinate of the earthquak was 22.001° N and 95.925° E as the latitude and longitude, respectively. The main earthquake (M_w 7.7) had some aftershocks that the strongest of them had a magnitude of 6.7.

The earthquake's shallow hypocenter and strike-slip mechanism produced peak ground velocities of 120 cm/s near Mandalay, as inferred from InSAR data[1]. Coulomb stress transfer modeling indicates increased seismic risk in adjacent fault segments, particularly the northern Sagaing Fault near Bhamo—a finding consistent with Stein et al. (1992)'s stress interaction theories[15-16].

In this study, the main objective is to utilize satellite-based Interferometric Synthetic Aperture Radar (InSAR) data from the Sentinel-1 platform to accurately map and quantify the surface deformation caused by the earthquake. The process involves acquiring pre- and post-event SAR images, generating interferograms, and analyzing ground displacement patterns along the Sagaing Fault. The results are used to characterize the rupture extent, slip distribution, and maximum displacement, providing essential data for seismic hazard assessment and supporting disaster response and reconstruction efforts.

2. Methodology

2.1. Data acquisition

This study employs Sentinel-1 satellite data, developed by the European Space Agency (ESA), to determine the displacement field caused by the 28 March 2025 Myanmar earthquake using InSAR techniques. Sentinel-1 satellites operate in both ascending and descending orbits, capturing radar images of the Earth's surface at revisit intervals of 12 days, reduced to 6 days with the launch of a second satellite. The radar images used are Single Look Complex (SLC) products acquired in Interferometric Wide (IW) mode. Both ascending and descending images were processed separately using the SNAP software, an open-source tool developed by ESA for Sentinel data analysis[17-20].

Table1 represents the characteristics of processed satellite images.

Table 1. Characteristics of satellite images used for this study

Polarization	Orbit Number	Orbit Mode	Image Type	Beam	Acquisition Date	Sensor
VV	58417	Ascending	SLC	IW	22/03/2025	Sentinel-1A
VV	58592	Ascending	SLC	IW	03/04/2025	Sentinel-1A

2.2. Interferogram creation

To ensure suitability for interferometric analysis, the coherence between image pairs was calculated. Coherence values was 0.97, indicating high image quality for displacement mapping. The images were then co-registered to guarantee that each pixel corresponds to the same ground feature.

Interferograms are generated by multiplying the first image with the complex conjugate of the second, allowing phase difference estimation for each pixel. The resulting interferogram displays displacement as colored fringes, where each fringe corresponds to half the radar wavelength ($\lambda/2$). For Sentinel-1 C-band images with a wavelength of 56 mm ($\lambda = 56$ mm), each fringe in the interferogram represents a displacement of 28 mm.

The measured phase difference (Φ_{Int}) includes contributions from topography, deformation, atmospheric effects, satellite orbit errors, and noise:

$$\Phi_{Int} = \Phi_{Topo} + \Phi_{Def} + \Phi_{Atm} + \Phi_{Orb} + \Phi_{Noise} \quad (1)$$

To determine the phase component of deformation, other components of the interferogram phase should be removed. For this purpose, the topographic phase was removed using the SRTM (3 arc-second, 90 m spatial resolution) DEM. The Goldstein filter was applied to reduce noise and enhance fringe visibility.

2.3. Phase unwrapping

Since phase values are wrapped within [0, 2π], phase unwrapping was performed using the Snaphu algorithm (Chen and Zebker, 2001) to retrieve the total phase of displacement over the acquisition interval.

In summary, this methodology integrates Sentinel-1 ascending SLC images, advanced interferometric and geocoding processing to accurately map the earthquake-induced displacement field, following best practices established in recent scientific literature[21-25].

In this study, given the importance of analyzing ground displacement for monitoring and assessing earthquake-induced damages, the displacement caused by the 28 March 2025 earthquake in Myanmar (Burma) was estimated. Two Sentinel-1A images were selected for this purpose, acquired on 22 March and 03 April 2025 in ascending orbit (**Table 1**)[26-32].

After initial processing and interferogram formation, phase unwrapping was performed using the Snaphu method to estimate the total deformation phase .The derived phase was then converted to line-of-sight (LOS) displacement using the following formula:

$$d = -\frac{\lambda}{4\pi}\Delta\phi_d \quad (1)$$

where:

d = LOS displacement between processed images

$\Delta\phi_d$ = unwrapped phase difference

λ = wavelength of Sentinel-1's C-band microwave signal

2.4. LOS Displacement map

To generate displacement maps, unwrapped phase values from interferograms must be converted using Equation 4. The interpretation of positive/negative phase values depends on master/slave image selection. When using the earlier acquisition as the master:

- Positive phase values indicate subsidence (target moving away from the satellite)
- Positive displacement values (enabled by the negative sign in Equation 4) represent uplift

This sign convention resolves interpretation conflicts between phase maps and displacement results. Using the secondary image as a master would eliminate this apparent contradiction in interferogram interpretation.

3. Results and discussions

The SAR pixel offset deformation field of this earthquake has been opened to the public through the National Earthquake Prevention and Disaster Reduction Public Service Platform [53].

Figure 2 displays an interferogram of the Myanmar earthquake. The image illustrates ground deformation patterns, where each full color cycle (fringe) represents half a wavelength of displacement (approximately 28 mm) in the satellite's line of sight. Concentric or closely spaced fringes indicate areas of significant deformation, potentially near the fault rupture. The colors represent phase differences, showing the magnitude and direction of ground movement. Areas with more fringes suggest greater deformation,

while uniform colors suggest less movement. The overall pattern helps to visualize the spatial extent and intensity of the earthquake's impact on the Earth's surface.

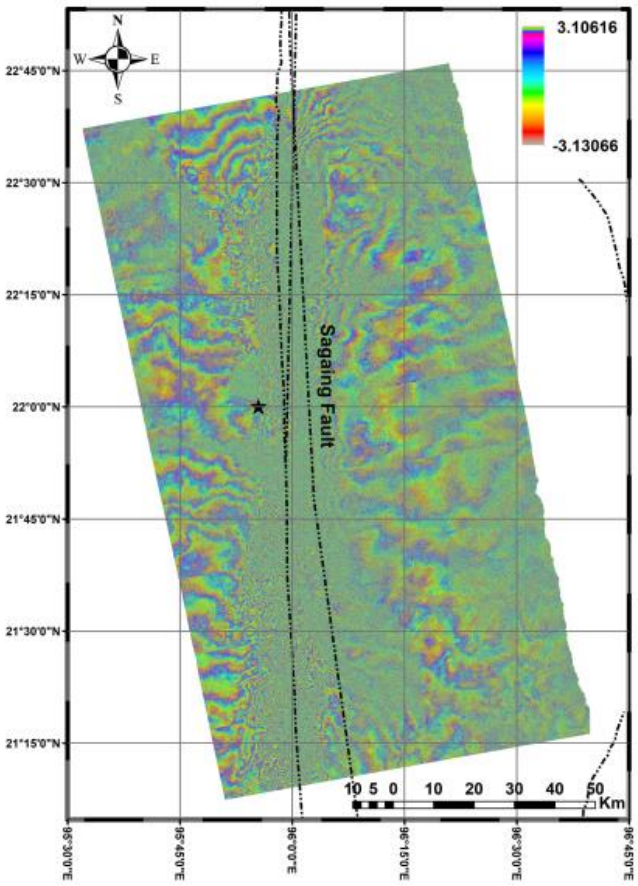

Figure 2. Interfrogram resulted from ascending images (23 March and 03 April) at the study area. Black dash line shows the Sagaing fault.

The interferogram displays fringes, each cycle representing approximately 28 mm (half the Sentinel-1 wavelength) of displacement in the satellite's line of sight (LOS). Fringe density indicates deformation magnitude; closer fringes suggest greater deformation. So:

- **Deformation Zones:** Closely spaced fringes, particularly along the central axis, indicate significant deformation, potentially exceeding several centimeters.
- **Spatial Extent:** The deformation extends roughly from 21°30'N to 22°30'N, covering a distance of approximately 110 km along the fault line.
- **Qualitative Displacement:** Colors cycle through the spectrum, representing phase changes from -π to +π radians.

Figure 3 illustrates a multi-look interferogram of the Myanmar earthquake zone. This technique reduces noise by averaging several pixels, resulting in a clearer deformation pattern. Each fringe represents approximately half a wavelength of displacement in the satellite's line of sight. The smoother color transitions, compared to single-look interferometry, enhance the visibility of broader deformation trends. Densely packed fringes still indicate areas of significant surface deformation, likely near the fault line, while larger, more uniform areas suggest stable regions. The multi-looking process helps in better visualizing regional deformation patterns by suppressing local variations and noise.

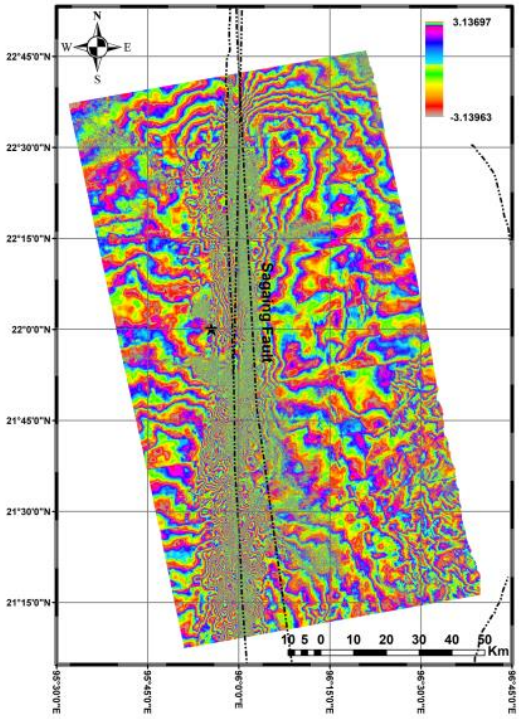

Figure 3. The ascending Interferogram created by images (23 March and 03 April) at the study area in Multilook mode (ML 6.2).

Multi-looking reduces noise, improving the clarity of deformation patterns. Each fringe still represents approximately 28 mm of LOS displacement [33-36]. The results show that:

- **Noise Reduction:** Smoother color transitions enhance the visibility of regional deformation trends.
- **Fault Line:** Persistent high-density fringes along the fault line confirm significant deformation.
- **Regional Stability:** Uniform areas suggest minimal displacement, generally less than 28 mm within each fringe.

Figure 4 shows an unwrapped interferogram of the Myanmar earthquake area. Unlike wrapped interferograms, where phase cycles are ambiguous, this image shows continuous phase values, directly proportional to the ground displacement in the satellite's line of sight [38-40]. The color scale indicates the magnitude of displacement, with different colors representing specific amounts of movement. This allows for a quantitative assessment of deformation, distinguishing areas of uplift (positive values) from subsidence (negative values). The absence of phase cycles simplifies interpretation, providing a clear map of the spatial distribution and magnitude of ground deformation caused by the earthquake.

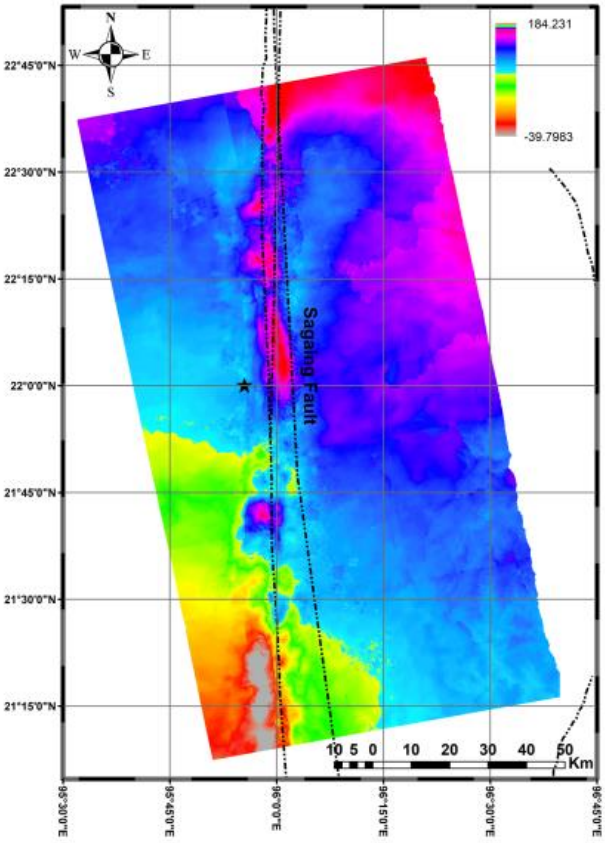

Figure 4. Unwrapped interferogram in the ascending orbit of the satellite.

The unwrapped interferogram shows continuous phase values, directly proportional to ground displacement in the satellite's LOS. The phase displacement ranges from approximately -39.8 to 184.2. **Figure 5** shows the displacement map resulting from the Myanmar earthquake. The displacement map quantifies ground displacement along the line of sight of satellite[40-43]. The color scale ranges from approximately -0.82 to 0.18 meters[44-47]. According to this map, the following expressions have resulted:

- **Uplift and Subsidence:** Areas in red show uplift up to 0.18 meters, while blue areas show subsidence down to -0.82 meters.
- **Maximum Displacement:** Maximum subsidence (-0.82 m) occurs at approximately 22.00° N, 96°00' E.
- **Deformation Distribution:** Uplift is concentrated in the northern part of the mapped area, with subsidence dominating the southern part.

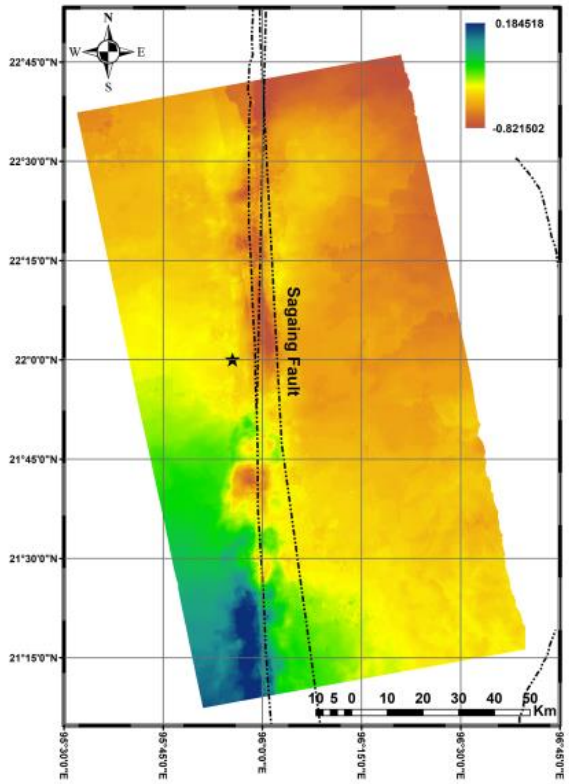

Figure 5. Surface displacement measured in the 28 March 2025 Myanmar earthquake (Mw 7.7) in LOS of ascending staellite orbite.

InSAR is a powerful tool for measuring ground displacement but has notable limitations, especially its inability to directly measure north-south displacement components due to the near-polar orbit of satellites like Sentinel-1. This limitation restricts the full three-dimensional (3D) characterization of surface deformation, as InSAR primarily captures displacements in the satellite's line-of-sight and azimuth directions, which are more sensitive to east-west and vertical movements. Additionally, InSAR faces challenges such as temporal and geometric decorrelation, atmospheric delays, and limited sensitivity to rapid or large displacements, which can degrade accuracy and coherence.

To overcome these constraints, future research could focus on integrating InSAR data with other geodetic techniques such as Global Navigation Satellite System (GNSS) measurements, which provide complementary 3D displacement information.

Advanced inversion methods like Tikhonov regularization and least-squares variance component estimation have shown promise in improving the retrieval of 3D displacement fields by combining range and azimuth measurements and assigning appropriate weights to heterogeneous datasets, enhancing precision by up to 80%. Moreover, the use of higher-resolution satellite data and multi-angle acquisitions from different satellite missions could improve sensitivity to north-south displacement components and reduce geometric limitations. Combining different satellite sensors with varying orbital geometries and revisiting times may also mitigate temporal decorrelation and improve monitoring of rapid ground movements. Overall, integrating multi-sensor data and advanced processing techniques represents a promising direction to address InSAR’s inherent limitations and enhance its capability for comprehensive earthquake deformation analysis.

4. Conclusion

The 28 March 2025 Myanmar earthquake (Mw 7.7) presented a significant seismic event along the Sagaing Fault, causing widespread devastation and providing crucial insights into the region's tectonics. This study utilized Interferometric Synthetic Aperture Radar (InSAR) techniques, employing Sentinel-1 satellite data to map and quantify the surface deformation resulting from the earthquake. The InSAR analysis provides a detailed understanding of the earthquake's impact, complementing ground-based observations and contributing to comprehensive seismic hazard assessments.

The interferogram (**Figure 2**) clearly illustrates the ground deformation patterns, with each fringe representing approximately 28 mm of displacement in the satellite's line of sight. The unwrapped interferogram (**Figure 4**) offers a quantitative assessment of the deformation, revealing continuous phase values directly proportional to ground displacement. The integration of these InSAR results with macroseismic data provides a comprehensive understanding of the earthquake's impact.

This InSAR-based study of the March 2025 Myanmar earthquake offers critical insights into the region's seismic activity. The results provide a detailed characterization of the rupture extent, slip distribution, and maximum displacement, essential for seismic hazard assessment and risk mitigation. The integration of these findings with other datasets can improve models, enhance early warning systems, and support long-term resilience planning, reducing the impact of future seismic events in this vulnerable region. This study underscores the importance of satellite-based remote sensing techniques in monitoring and assessing earthquake-induced deformation, providing valuable information for scientific research and disaster management.

Conflict of interest

The authors declare no conflict of interest.

References

1. Tiongson, S. F., & Ramirez, R. (2022). Mapping of ground surface deformations and their associated damage using SAR interferometry: a case study of the 2020 Masbate earthquake. In E3S Web of Conferences (Vol. 347, p. 03014). EDP Sciences.
2. Bayramov, E., Buchroithner, M., Kada, M., & Zhuniskenov, Y. (2021). Quantitative assessment of vertical and horizontal deformations derived by 3d and 2d decompositions of InSAR line-of-sight measurements to supplement industry surveillance programs in the Tengiz oilfield (Kazakhstan). Remote Sensing, 13(13), 2579.
3. Huang, W., Mei, X., Wang, Y., Fan, Z., Chen, C., & Jiang, G. (2022). Two-dimensional phase unwrapping by a high-resolution deep learning network. Measurement, 200, 111566.
4. Emadali, Lotfollah, Mahdi Motagh, and Mahmud Haghshenas Haghighi. 2017. "Characterizing Post-Construction Settlement of the Masjed-Soleyman Embankment Dam, Southwest Iran, Using TerraSAR-X SpotLight Radar Imagery." : Engineering Structures 143 (2017) 261–273.
5. Funning, G. J., & Garcia, A. (2019). A systematic study of earthquake detectability using Sentinel-1 Interferometric Wide-Swath data. Geophysical Journal International, 216(1), 332-349.
6. Nuangnun, C., Phuengkum, N., Srikongrug, S., Mameechai, D., Thongperm, P., & Nuleg, W. (2018). Earthquake trends in Thailand and Myanmar. ASEAN Journal of Scientific and Technological Reports, 21(3), 167-173.
7. Fernandez, G., Tun, A. M., Okazaki, K., Zaw, S. H., & Kyaw, K. (2018). Factors influencing fire, earthquake, and cyclone risk perception in Yangon, Myanmar. International journal of disaster risk reduction, 28, 140-149.
8. Shiddiqi, H. A., Tun, P. P., Kyaw, T. L., & Ottemöller, L. (2018). Source study of the 24 August 2016 Mw 6.8 Chauk, Myanmar, earthquake. Seismological Research Letters, 89(5), 1773-1785.
9. Wang, M., Shen, Z. K., Wang, Y. Z., Bürgmann, R., Wang, F., Zhang, P. Z., ... & Xue, L. (2021). Postseismic deformation of the 2008 Wenchuan earthquake illuminates lithospheric rheological structure and dynamics of eastern Tibet. Journal of Geophysical Research: Solid Earth, 126(9), e2021JB022399.
10. Kreemer, C., Hammond, W. C., & Blewitt, G. (2018). A robust estimation of the 3-D intraplate deformation of the North American plate from GPS. Journal of Geophysical Research: Solid Earth, 123, 4388–4412.

11. Lindsey, E. O., Wang, Y., Aung, L. T., et al. (2023). Active subduction and strain partitioning in western Myanmar revealed by a dense survey GNSS network. Earth and Planetary Science Letters, 622, 118384.
12. Wang Y Z, Zhang Z, Zhang X, et al. Rapid estimation of parameters related to the 28 March 2025 M7.9 earthquake in Myanmar[J]. Progress in Earthquake Sciences, 2025, 55(5): 284-289. DOI: 10.19987/j.dzkxjz.2025-037
13. Fadil, W., Wei, S., Bradley, K., Wang, Y., He, Y., Sandvol, E., ... & Htwe, Y. M. M. (2023). Active faults revealed and new constraints on their seismogenic depth from a high-resolution regional focal mechanism catalog in Myanmar (2016–2021). Bulletin of the Seismological Society of America, 113(2), 613-635.
14. Howard, S., & Krishna, G. (2025). Myanmar junta blocking aid as earthquake death toll nears 3000.
15. Tiongson, S. F., & Ramirez, R. (2022). Mapping of ground surface deformations and its associated damage using SAR interferometry: a case study of the 2020 Masbate earthquake. In E3S Web of Conferences (Vol. 347, p. 03014). EDP Sciences.
16. Wang, Y., Sieh, K., Tun, S. T., Lai, K. Y., & Myint, T. (2014). Active tectonics and earthquake potential of the Myanmar region. Journal of Geophysical Research: Solid Earth, 119(4), 3767-3822.
17. Thein, M., Myint, T., Tun, S. T., & Swe, T. L. (2009). Earthquake and tsunami hazard in Myanmar. Journal of Earthquake and Tsunami, 3(02), 43-57.
18. Rajaram, C., Vemuri, J. P., & Singhal, S. Seismological Features and Preliminary Damage Assessment of the Devastating March 28, 2025 Myanmar Earthquake: A Comprehensive Overview. Available at SSRN 5219429.
19. Wibowo, A. (2025). Modeling Potential Earthquake Risk Zones in Myanmar Due to the March 2025 Earthquake and Geological Factors Using Machine Learning.
20. Fadil, W., Lindsey, E. O., Wang, Y., Maung, P. M., Luo, H., Swe, T. L., ... & Wei, S. (2021). The January 11, 2018, Mw 6.0 Bago-Yoma, Myanmar earthquake: A shallow thrust event within the deforming Bago-Yoma Range. Journal of Geophysical Research: Solid Earth, 126(7), e2020JB021313.
21. Ko, S. C., & Swe, T. L. SEISMOTECTONICS INVESTIGATION IN YANGON REGION, MYANMAR.
22. Pailoplee, S., Channarong, P., & Chutakositkanon, V. (2013). Earthquake Activities in the Thailand-Laos-Myanmar Border Region: A Statistical Approach. Terrestrial, Atmospheric & Oceanic Sciences, 24(4).
23. Eftekhari, N. , Motaghed, S. , Emadali, L. and Sayyadpour, H. (2025). Artificial Statistical Method to Estimating Seismicity Parameters for Ahvaz City Using a Stochastic Synthetic Seismic Catalog. *Journal of Seismology and Earthquake Engineering*, (), -.
doi: 10.48303/jsee.2025.2041574.1124
24. Motaghed, S. and fakhriyat, A. reza (2025). Uncertainties in seismic hazard assessment of Metropolitan Tehran. *International Journal of Reliability, Risk and Safety: Theory and Application*, (), -.
doi: 10.22034/ijrrs.2024.494580.1179
25. Motaghed, sasan, Emadali, Loftollah, (2025). Performance-Based Methodology for Seismic Design and Evaluation of Bridges, *Advance Researches in Civil Engineering*,
10.30469/arce.2025.511561.1084
26. motaghed, sasan, shabaneh, mohammad hossein, ghasemi golsorkhdan, mehran, mohammadi, mehdi, Schmidt hammer test for estimating concrete strength; Calibration and Calibration, *Advance Researches in Civil Engineering* 10.30469/arce.2025.504865.1083
27. Lotfollah Emadali, Mozhgan Mehrpak, Sasan Motaghed, Nasrollah Eftekhari, Determination of displacement components of Sisakht earthquake (M 5.4) by Radar Interferometry (InSAR), Bulletin of Earthquake Science and Engineering – BESE,
10.48303/bese.2025.2036596.1193
28. Abiari A, Motaghed S, Sayyadpour H, et al. Seismic fragility evaluation of box deck concrete bridge equipped with shape memory alloy under bi-directional earthquake loading. Earthqauke2025;3(1):8253.
http://doi:10.59429/ear.v3i1.8253
29. Motaghed S, shamsizadeh M, eftekhari N. Earthquake possibility space of Ahvaz city based on intuitionistic fuzzy theory. Journal of Engineering Geology 2024; 18 (3) :320-340
30. http://jeg.khu.ac.ir/article-1-3126-fa.html
https://doi: 10.30469/arce.2024.476684.1079
31. Motaghed, S., Mahmoodian, H., ri, S. (2024). Case Studies in Seismic Risk Assessment of Masonry Fire Station Buildings. *International Journal of Reliability, Risk and Safety: Theory and Application*, *7*(2), 40-51. doi: 10.22034/IJRRS.2024.7.2.4
https://doi: 10.22034/ijrrs.2024.471909.1169
32. Motaghed, S., & Mehrabi Moghaddam, A. (2024). Confidence level for Iranian Existing Moment Resisting RC Structures Based on Demand and Capacity Factored Design Method. *International Journal of Reliability, Risk and Safety: Theory and Application*, *7*(1), 93-102.
https://doi: 10.22034/IJRRS.2024.7.1.11

33. Motaghed, S., Mohammadi, M., Eftekhari, N., Khazaea, M,. SCP parameters estimation for catalogs with uncertain seismic magnitude values. Acta Geophys. (2024). https://doi.org/10.1007/s11600-024-01404-5
34. Fakhriyat, A., Motaghed,. S & Shahidzadeh, M. S. (2024). The necessity of modeling the column beam joint panel zone in reinforced concrete structures with behavioral degradation. *Amirkabir Journal of Civil Engineering*, *56*(7), 3-3. https://doi: 10.22060/ceej.2024.22089.7900
35. Eftekhari N, Motaghed S, Emadali L, Sayyadpour H. Ranking of ground motion prediction equation for use in the seismic hazard analysis of Ahvaz city using data envelopment analysis. Journal of Engineering Geology 2022; 16 (2) :99-124 http://jeg.khu.ac.ir/article-1-3083-fa.html
36. Motaghed, S., Eftekhari, N., Emadali, L., & Sayyadpour, H. (2024). Revision of Ahvaz City seismic hazard analyzes according to the state of Ahvaz fault. *Advanced Applied Geology*, (), -. https:// doi: 10.22055/aag.2024.44810.2405
37. Motaghed, S., nakhlian, A., emadali, L., eftekhari, N., & mahmoudian, H. (2023). Seismic hazard assessment using arithmetic-weighted overlay method based on earthquake potential index (EPI), the southwestern Iran. Iranian Journal of Remote Sensing & GIS, (), -. https:// doi: 10.48308/gisj.2023.229646.1133
38. Motaghed, S., Eftekhari, N., & Mohammadi, M, Khazaee, M.. (2023) Logic tree branches' weights in the probabilistic seismic hazard analysis; the need to combine inter-subjective and propensity probability interpretations, journal of seismology, https://doi.org/10.1007/s10950-023-10177-1
39. Motaghed, S., Eftekhari, N., khazaee, M., & yousefi Dadras, E. (2023). Selection and Ranking the Ground Motion Prediction Equations for Tehran Region. Journal of Structural and Construction Engineering, (), -. https:// doi: 10.22065/jsce.2023.393094.3088
40. Motaghed, S., Fakhriyat, A.R., A reliable method for determining the tapered minimum magnitude in a probabilistic seismic hazard analysis, International Journal of Reliability, Risk and Safety: Theory and Application https:// doi: 10.30699/IJRRS.5.2.9
41. Motaghed, S., Khazaee, M., Eftekhari, N., & Mohammadi, M. (2023). A non-extensive approach to probabilistic seismic hazard analysis. Natural Hazards and Earth System Sciences, 23(3), 1117-1124. https://doi.org/10.5194/nhess-23-1117-2023
42. Motaghed, S., nakhlian, A., emadali, L., eftekhari, N., & mahmudian, H. (2023). Determining the natural frequency of Behbahan city soil using microtremor data analysis. Journal of Geography and Environmental Hazards, (), -. https:// doi: 10.22067/geoeh.2023.80563.1326
43. barzian, V., Motaghed, S., Mehrabi Moghaddam, A., Asghari Pari, S. A., & emadali, L. (2022). Investigation the effect of structural parameters uncertainty on the response of incremental dynamic analysis of intermediate steel moment resisting frame structures. Journal of Structural and Construction Engineering, 9(10), 175-195. https:// doi: 10.22065/jsce.2022.311616.2612
44. Mehrabi Moghadam, A., Yazdani, A., Motaghed, S. (2022). Considering the Yielding Displacement Uncertainty in Reliability of Mid-Rise R.C. Structures. Journal of Rehabilitation in Civil Engineering, 10(3), 141-157. https:// doi: 10.22075/jrce.2021.19660.1376
45. Motaghed, S., Khazaee, M. & Mohammadi, M. The b-value estimation based on the artificial statistical method for Iran Kope-Dagh seismic province. Arab J Geosci 14, 1461 (2021). https://doi.org/10.1007/s12517-021-07970-y
46. Motaghed, S., & fakhriyat, A. R. (2021). Modeling inelastic behavior of RC adhered shear walls in opensees. Journal of Modeling in Engineering, 18(63), 15-25. https:// doi: 10.22075/jme.2020.18042.1740
47. Moradi Tayebi F, motaghed S, Dastanian R. Evaluation Chaotic Behavior and Time Series Prediction of Tehran Earthquakes. MCEJ 2020; 20 (3) :147-160 http://mcej.modares.ac.ir/article-16-15687-fa.html
48. Nicknam A., Khanzadi M., Motaghed S., Yazdani A. (2017) Applying b-value statistical variation to seismic hazard analysis, Indian Journal of Geo-Marine Sciences: 46; 391-396
49. Motaghed, S., yazdani, A., nicknam, A., & khanzadi, M. (2018). Sobol sensitivity generalization for engineering and science applications. Journal of Modeling in Engineering, 16(54), 217-226. https:// doi: 10.22075/jme.2017.12259.1221
50. Yazdani, A., Motaghed, S., & Mehrabi Moghadam, A. (2016). Evaluation of Seismic Risk Effect on Total Reliability Index of Structures, Case Study of Concrete Flexible Frame Frames. Asas Journal, 18(43), 26-37.
51. Motaghed S., khooshecharkh A., 2011, Damage–Based Optimal Longitudinal Reinforcement for RC frames, European Journal of Scientific Research, Vol.50, Issue 2, P.191-201

52. Motaghed S. ,khooshecharkh A., 2011, Probabilistic Evaluation of the Effects of Concrete Compression Strength on the Reinforced Concrete Building Damageability , European Journal of Scientific Research, Vol. 50 Issue 2, p.202-207
53. Motaghed S., Shahidzade M.S.,2011, seismic evaluation of steel I- girder bridges , Journal of Applied Sciences Vol. 11, Issue 1, p. 104-110
https://www.earthquake.ac.cn/monitor/productInfo/4612